R. & M. No. 3004
(17,423)
A.R.C. Technical Report

MINISTRY OF SUPPLY

AERONAUTICAL RESEARCH COUNCIL
REPORTS AND MEMORANDA

The Interaction between Shock Waves and Boundary Layers at the Trailing Edge of a Double-Wedge Aerofoil at Supersonic Speed

By
B. D. HENSHALL, B.Sc., and R. F. CASH, A.F.R.Ae.S.,
of the Aerodynamics Division, N.P.L.

LONDON: HER MAJESTY'S STATIONERY OFFICE
1957
PRICE 3s. 6d. NET

The Interaction between Shock Waves and Boundary Layers at the Trailing Edge of a Double-Wedge Aerofoil at Supersonic Speed

By

B. D. HENSHALL, B.Sc., and R. F. CASH, A.F.R.Ae.S.,
of the Aerodynamics Division, N.P.L.

COMMUNICATED BY THE DIRECTOR-GENERAL OF SCIENTIFIC RESEARCH (AIR),
MINISTRY OF SUPPLY

Reports and Memoranda No. 3004*
March, 1955

1. *Summary and Introduction.*—A comprehensive review of the work at the National Physical Laboratory on shock-wave—boundary-layer interaction has recently been published[1]. The experiments reported below were designed to investigate a further case of this interaction which was not considered in Ref. 1; namely, that occurring near the trailing edge of a double-wedge aerofoil at supersonic speed. This interaction should be similar to that where the shock is generated by a wedge attached to a flat plate; indeed, the only difference between these two cases is that the downstream solid boundary of the latter is replaced by the centre-line of the wake of the aerofoil. Experimental results confirm that these interactions are both qualitatively and quantitatively similar and further support the physical explanations of these flow patterns given in Ref. 1; moreover, the results apply generally to aerofoils with flat surfaces towards the rear.

2. *Experimental Data.*—Supersonic liners, nominally $M_0 = 1 \cdot 60$, have recently been designed for the 20-in. × 8-in. High-Speed Wind Tunnel at N.P.L. These liners have not been calibrated† to date, but this is unnecessary provided that the Mach number is uniform. The Mach number M immediately upstream of the interaction (that is, the Mach number of the flow between the shoulder and the trailing edge of the wedge) depends only on the angle of incidence of the wedge α and the true free-stream Mach number M_0. It was found that the pressure distributions on the aerofoil (*see* Fig. 1) behaved as if $M_0 = 1 \cdot 608$, corresponding flow deflections θ, from standard tables[2], giving the observed pressures if it was assumed that $\theta = 0$ deg when $M = 1 \cdot 608$. The included angle τ of the symmetrical double-wedge aerofoil was 12 deg, the model chord 2 in. and the span 8 in. Simple geometry gives the relation

$$\theta = \alpha + \tfrac{1}{2}\tau = \alpha + 6 \text{ deg} \qquad \text{(1)}$$

between the flow deflection θ and the incidence of the aerofoil α.

---

* Published with the permission of the Director, National Physical Laboratory.

† It is, however, known that the resultant flow is free from pressure gradients large enough to affect the present results.

Seven pressure holes were equally spaced on the aerofoil from $0 \cdot 65c$ to $0 \cdot 95c$ in $0 \cdot 05c$ steps; alternate holes were located 1 in. on either side of the aerofoil span centre-line. At the $0 \cdot 60c$ position two holes were provided, each $\frac{1}{2}$-in. from the centre-line, as a check on possible spanwise effects in the flow over the aerofoil. A trailing-edge hole was not provided in the model.

Two cases of the interaction of the trailing-edge shock with the boundary layer on the aerofoil were considered; namely, those when the state of the boundary layer was (*a*) laminar and (*b*) turbulent. In the latter case, transition was artificially produced by layers of carborundum, approximately 5 thousandths of an inch thick, on the first $0 \cdot 1$ chord of both surfaces of the aerofoil.

All the pressure distributions obtained are given in Fig. 1; values for the turbulent case (Fig. 1b) for $\theta < 11$ deg are identical to those of the laminar case (Fig. 1a), save that separation is not present near the trailing edge of the wedge. Values of θ greater than 15 deg could not be obtained because the tunnel became choked. It may also be noted that $\theta = 15$ deg would be expected to lead to detachment of the leading-edge shock wave, and, further, consideration of the load on the model and its supports (slots cut in the $1\frac{1}{2}$-in. thick windows of the tunnel) would restrict θ to a value just above 15 deg in any case.

3. *Analysis of Results*.—(*a*) *Boundary Layer Laminar on Aerofoil, but Turbulent on Reattachment to Wake*.—Fig. 2a is a direct-shadow photograph of this case. The characteristic 'laminar line' is visible near the wedge surface, whilst the wake is clearly turbulent. Methods of analysis used in Ref. 1 have been applied to the results of these investigations. For each test where separation has occurred on the aerofoil, the upstream influence d/δ_0^* was calculated in the following manner. The upstream distance d is defined as the distance from the trailing edge of the aerofoil to the point O where the local static pressure p effectively begins to depart from p_1, the static pressure acting on the surface of the wedge when separation is absent (*see* Fig. 1). This point O is arbitrarily defined as the position where $p = 1 \cdot 02 p_1$. The displacement thickness δ_0^* is calculated *via* the Reynolds number R_0 of the test; further, it is assumed that x_0 (on which R_0 is based) is the distance from the leading edge of the wedge to the point O, that is $(2 - d)$ in. An approximate straight line relation between the Reynolds and Mach numbers of isentropic flow, valid for the Mach number range $1 \cdot 65 < M < 2 \cdot 15$ is (from data given in graphs[2])

$$\frac{R_0}{10^6 x_0} = \left(\frac{7 \cdot 34 - 1 \cdot 6M}{12}\right) \quad \ldots \quad (2)$$

where atmospheric stagnation conditions are assumed for the flow ($T_0 = 10$ deg C), and x is measured in inches. Further, the displacement thickness δ_0^* as given by Young[4] is

$$\delta_0^* = 1 \cdot 72(1 + 0 \cdot 277M^2)\frac{x_0}{\sqrt{R_0}} \quad \ldots \quad (3)$$

which becomes, on substituting for R_0,

$$\frac{\delta_0^*}{x_0^{1/2} 10^{-3}} = 1 \cdot 72(1 + 0 \cdot 277M^2) \Big/ \left(\frac{7 \cdot 34 - 1 \cdot 6M}{12}\right)^{1/2} . \quad \ldots \quad (4)$$

The precise value of x_0 will not be $(2 - d)$ in. since the growth of the boundary layer will be affected by the *lower* Mach number upstream of the shoulder of the wedge and also by the 12 deg expansion round the shoulder.

However, the values of d/δ_0^* calculated in the above manner should not be widely different from their true values.

Since the static pressure in the wake of the aerofoil eventually returns to that in the undisturbed stream (*i.e.*, the value of p_1 for $\theta = 0$ deg), the overall pressure ratio across the interaction p_{max}/p_1 is given by the ratio of p_1 for $\theta = 0$ deg to p_1 for $\theta = \theta$ deg, and the corresponding pressure coefficient $C_{p\max}$ by

$$C_{p\max} = \frac{2}{\gamma M^2}\left(\frac{p_{\max}}{p_1} - 1\right). \qquad (5)$$

One further relation, which gives information about the 'laminar foot' of the interaction is

$$C_{pT} = \frac{2}{\gamma M^2}\left(\frac{p_T}{p_1} - 1\right), \qquad (6)$$

where p_T/p_1 is the pressure ratio at the top of the foot (*see* Fig. 1a, $\theta = 11$ deg and 12 deg).

(*b*) *Boundary Layer Turbulent over Whole Range of Interaction.*—Fig. 2 (*b*) is a direct-shadow photograph of this type of interaction. The analysis of results is precisely as before, but the formula for δ_0^* is that given by Monaghan[5], namely

$$\delta_0^* = \frac{0\cdot0475(1 + 0\cdot35M^2)}{\left(1 + 0\cdot88\,\frac{\gamma - 1}{2}\,M^2\right)^{0\cdot44}}\,\frac{x_0}{R_0^{1/5}}. \qquad (7)$$

Again, x_0 is supposed equal to $(2 - d)$ in., although this is clearly only approximately correct. The position of the beginning of the upstream effect has been arbitrarily defined as the point O where $p = 1\cdot05p_1$, since the pressure rise is more sudden in the turbulent case than in the laminar case.

4. *Discussion of Results.*—Fig. 3 presents comparison results for the two types of shock-wave–boundary-layer interaction discussed above and for the externally generated shock case[1], for (Fig. 3a) laminar layers and (Fig. 3b) turbulent layers. In each set of three schlieren photographs† the Reynolds number, Mach number and overall pressure-ratio coefficient across the region of interaction, $C_{p\max}$, are of the same order. It will be noted that, for either type of boundary layer, the double-wedge aerofoil case closely resembles the interaction occurring when the shock is generated by a wedge attached to a flat plate. An external shock wave causes a much greater upstream effect for a given $C_{p\max}$ than either of the other types of shock.

Analysis of results for $\theta = 11$ deg and $\theta = 12$ deg (Fig. 1a), where the 'laminar foot' is most pronounced, yields the data illustrated by Fig. 4. The curve of C_{pT} versus R_0 is taken from Ref. 1, and it is seen that very good agreement exists between this curve and the experimental points corresponding to the schlieren photographs reproduced herewith.

Finally, we must consider the flow deflection which will just cause flow separation. In Ref. 1 it was found that for the shock generated by the wedge on a plate

$$\theta_{sep}\ (\text{laminar case}) \simeq 4\ \text{deg}$$

$$\theta_{sep}\ (\text{turbulent case}) \simeq 12\ \text{deg}.$$

Since the double-wedge aerofoil had no trailing-edge hole, the direct determination of separation by divergence of the trailing-edge pressure[6] was not possible. Consequently the pressure distributions (Fig. 1) can only indicate very approximately the value of θ_{sep}. From Fig. 1a, θ_{sep} (laminar) $<$ 5 deg, and from Fig. 1b, θ_{sep} (turbulent) $<$ 14 deg. Fig. 5 suggests an approximate value of

† Data for (i) and (ii) supplied by Dr. G. E. Gadd of the N.P.L.

θ_{sep} (laminar) $\simeq 3 \cdot 8$ deg. This result is derived from a straight line plot of $C_{p\max}$ against $(d/\delta_0{}^*)(R/10^4)^{1/3}$, a factor which, according to Ref. 1, should be roughly independent of Reynolds number and hence a function only of shock strength and Mach number. Note also the good correlation between the present tests and those of Gadd *et al.* at $M = 2 \cdot 0$.

A series of schlieren photographs were taken at $\frac{1}{2}$ deg intervals in the ranges 4 deg $< \theta <$ 6 deg (laminar) and 11 deg $< \theta <$ 13 deg (turbulent), and specimen photographs of these series are reproduced as Fig. 6. From these photographs we may deduce that θ_{sep} (laminar) $<$ 5 deg, and θ_{sep} (turbulent) $< 12\frac{1}{2}$ deg. It is clear that a small separated region is present in Fig. 6a (ii) which is extended considerably in Fig. 6a (iii). The detection of turbulent separation is more difficult from the photographs, since the separated region is of very small extent. The occurrence of separation is therefore assumed to coincide with the formation of a slight 'neck' and an increase in thickness of the trailing-edge shock wave adjacent to the boundary layer. Sketches are also given in Fig. 6 to illustrate these features of the flow.

5. *Conclusions.*—The shock-wave–boundary-layer interaction occurring near the trailing edge of a double-wedge aerofoil at supersonic speed is qualitatively similar to that occurring when the shock is generated by a wedge attached to a plate. Both these phenomena show large differences of upstream effect from the interaction of an externally generated shock with boundary layers of the same type.

NOTATION

M_0	Tunnel free-stream Mach number
M	Mach number immediately upstream of the interaction; that is, the Mach number of the flow between the shoulder and the trailing-edge of the double-wedge aerofoil
θ	Flow deflection angle
τ	Total included angle of symmetrical double-wedge aerofoil
α	Incidence of aerofoil
c	Aerofoil chord
d	Upstream distance to point O from trailing edge of aerofoil. Point O defined in text
$\delta_0{}^*$	Calculated boundary-layer displacement thickness at point O
x_0	Distance from leading edge of aerofoil to point O
R_0	Reynolds number based on length x_0 and effective free-stream Mach number M
p	Local static pressure
p_1	Static pressure on surface of wedge corresponding to unseparated flow conditions
$p_{\max}$	Peak value of p attained at the wall in the region of interaction; equal to p_1 corresponding to $\theta = 0$ deg
p_T	p at 'top' of laminar foot (*see* Fig. 1)
C_p	Pressure coefficient $\frac{2}{\gamma M^2}\left(\frac{p}{p_1} - 1\right)$ where $\gamma = 1 \cdot 4$; suffixes corresponding to p

REFERENCES

No.	Author	Title, etc.
1	G. E. Gadd, D. W. Holder and J. D. Regan.	An experimental investigation of the interaction between shock waves and boundary layers. *Proc. Roy. Soc.*, Series A. Vol. 226. pp. 227 to 253. 1954.
2	L. Rosenhead *et al.*	A selection of tables for use in calculations of compressible airflow. Clarendon Press, Oxford. 1952.
		A selection of graphs for use in calculations of compressible airflow. Clarendon Press, Oxford. 1954.
3	D. W. Holder and R. J. North ..	Schlieren methods for observing high-speed flows. C.P. 167. July, 1953.
4	A. D. Young	Skin friction in the laminar boundary layer in compressible flow. *Aero. Quart.*, Vol. 1, p. 137. August, 1949.
5	R. J. Monaghan	Comparison between experimental measurements and a suggested formula for the variation of turbulent skin friction in compressible flow. C.P. 45. February, 1950.
6	D. W. Holder, H. H. Pearcey, G.E. Gadd and J. Seddon	The interaction between shock waves and boundary layers; with a note on the effects of the interaction on the performance of supersonic intakes. C.P. 180. February, 1954.

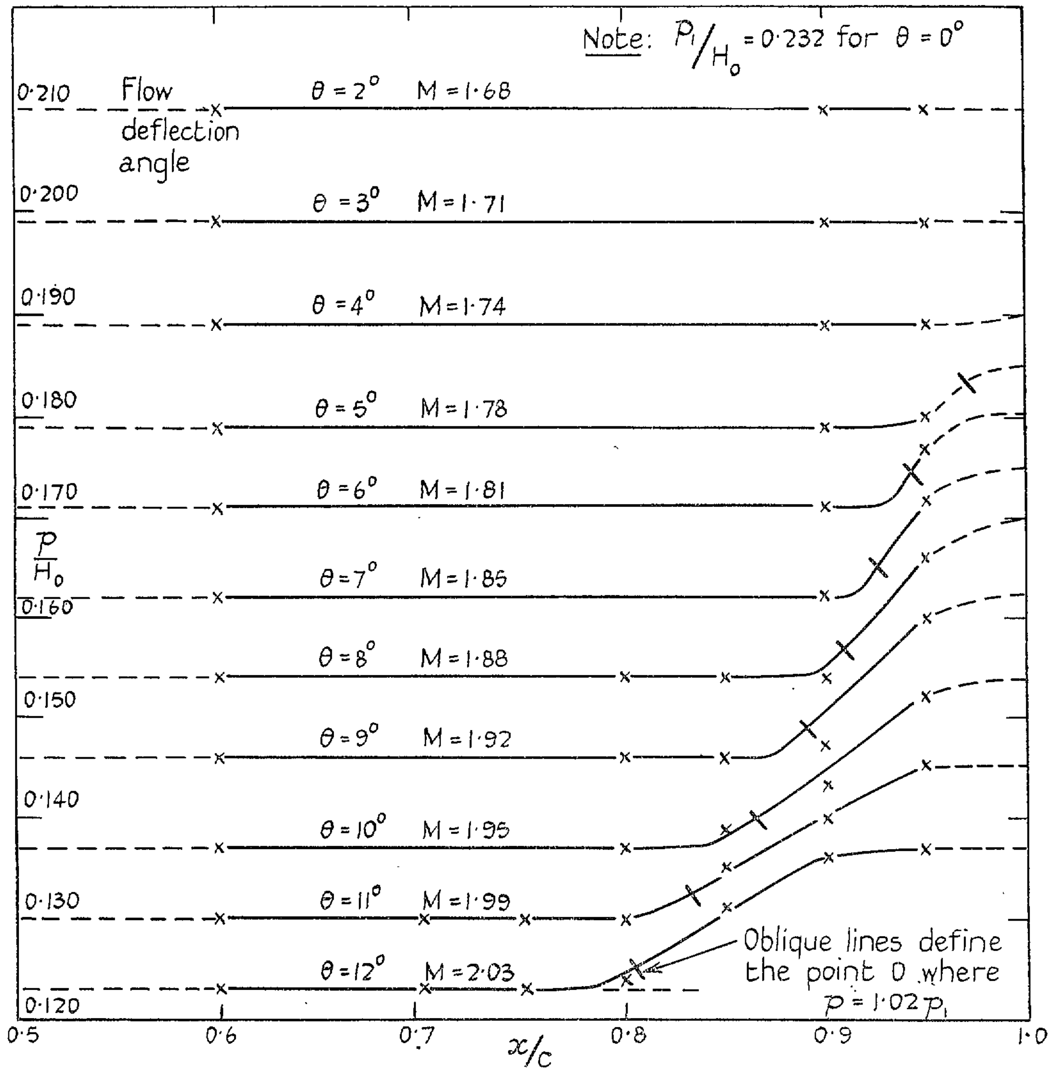

FIG. 1a. Laminar boundary layers.

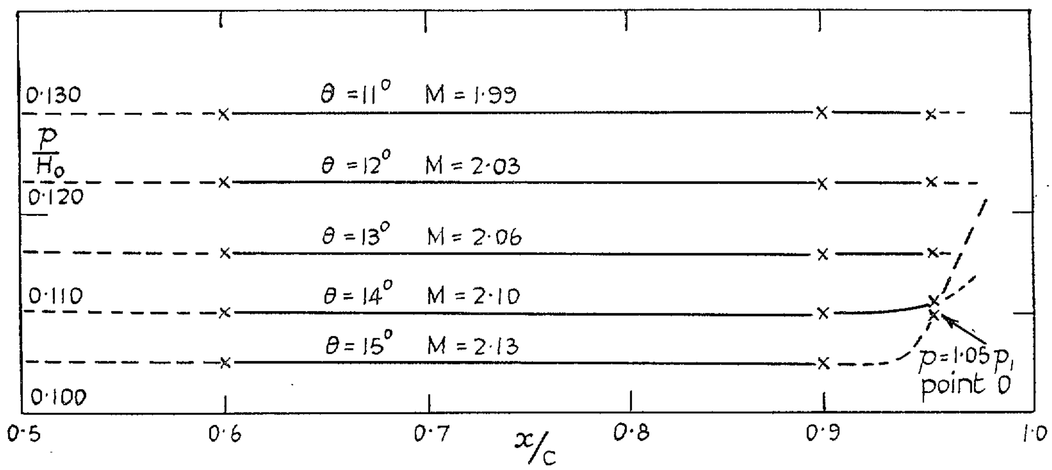

FIG. 1b. Turbulent boundary layers.

FIG. 1. Pressure distributions for 12-deg double-wedge aerofoil of 2-in. chord.

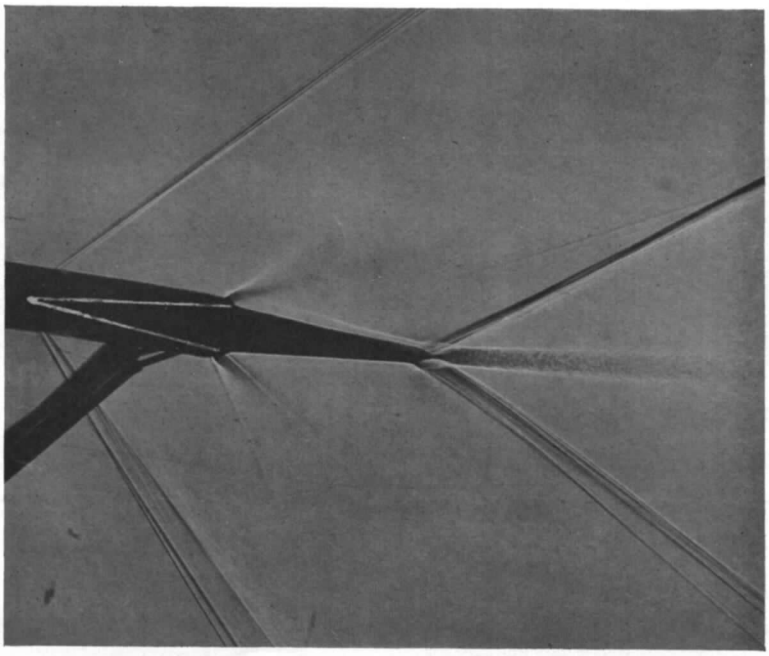

FIG. 2a. Laminar boundary layer on aerofoil, but turbulent on reattachment to wake. $\theta = 11$ deg. $M = 1\cdot99$.

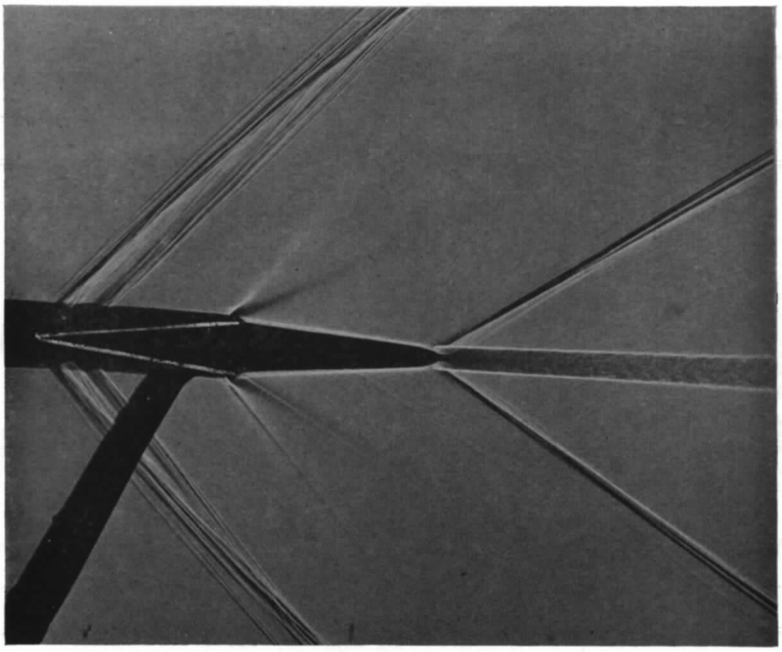

FIG. 2b. Turbulent boundary layer throughout whole range of shock-wave–boundary-layer interaction. $\theta = 6$ deg. $M = 1\cdot81$.

FIG. 2. 12-deg double-wedge aerofoil. Direct-shadow photographs showing state of the boundary layer during boundary-layer–shock-wave interaction.

FIG. 3a. Laminar boundary layers.

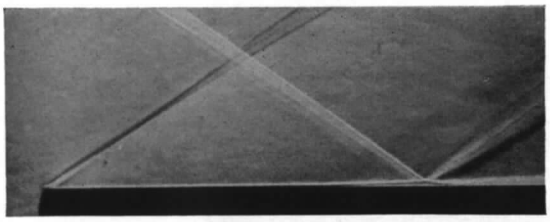

(i) External shock. $\theta = 5$ deg.

$R_0 = 4{\cdot}9 \times 10^5$. $M = 2{\cdot}0$.

$d/\delta^*_0 = 70$. $C_{p\,\max} = 0{\cdot}28$.

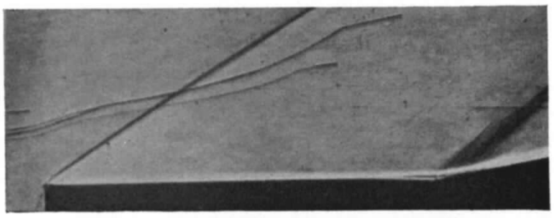

(ii) Shock generated by wedge on plate. $\theta = 10$ deg.

$R = 5{\cdot}4 \times 10^5$. $M = 2{\cdot}0$.

$d/\delta^*_0 = 27$. $C_{p\,\max} = 0{\cdot}25$.

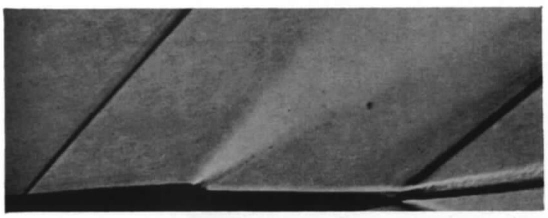

(iii) Double-wedge aerofoil. $\theta = 9$ deg.

$R = 6{\cdot}3 \times 10^5$. $M = 1{\cdot}92$.

$d/\delta^*_0 = 28$. $C_{p\,\max} = 0{\cdot}23$.

FIG. 3b. Turbulent boundary layers.

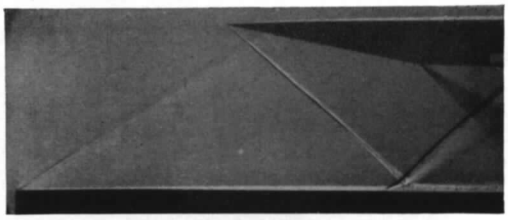

(i) External shock. $\theta = 8$ deg.

$R_0 = 8 \times 10^6$. $M = 2{\cdot}0$.

$d/\delta^*_0 = 28$. $C_{p\,\max} = 0{\cdot}43$.

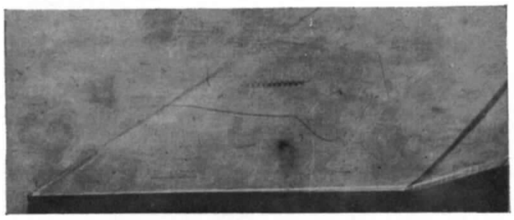

(ii) Shock generated by wedge on plate. $\theta = 15$ deg.

$R = 3{\cdot}7 \times 10^6$. $M = 2{\cdot}0$.

$d/\delta^*_0 = 9$. $C_{p\,\max} = 0{\cdot}45$.

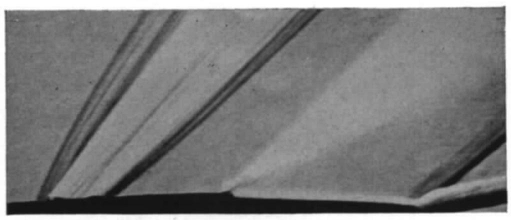

(iii) Double wedge aerofoil. $\theta = 15$ deg.

$R = 6{\cdot}3 \times 10^5$. $M = 2{\cdot}13$.

$d/\delta^*_0 = 8$. $C_{p\,\max} = 0{\cdot}40$.

FIG. 3. Types of shock-wave–boundary-layer interaction. Schlieren photographs.

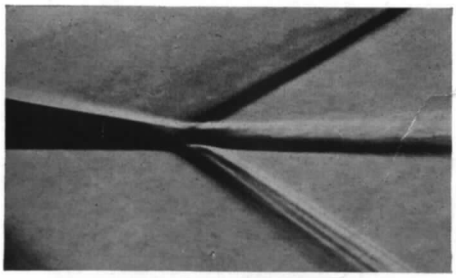

$M = 1{\cdot}99$. $R = 5{\cdot}8 \times 10^5$. $\theta = 11$ deg.
$d/\delta^*_0 = 42$. $C_{pT} = 0{\cdot}042$.

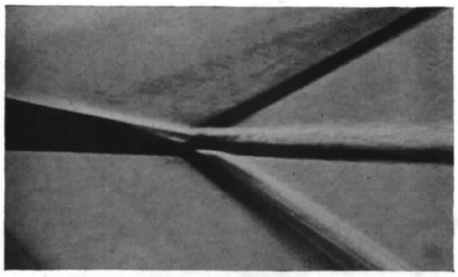

$M = 2{\cdot}03$. $R = 5{\cdot}5 \times 10^5$. $\theta = 12$ deg.
$d/\delta^*_0 = 49$. $C_{pT} = 0{\cdot}040$.

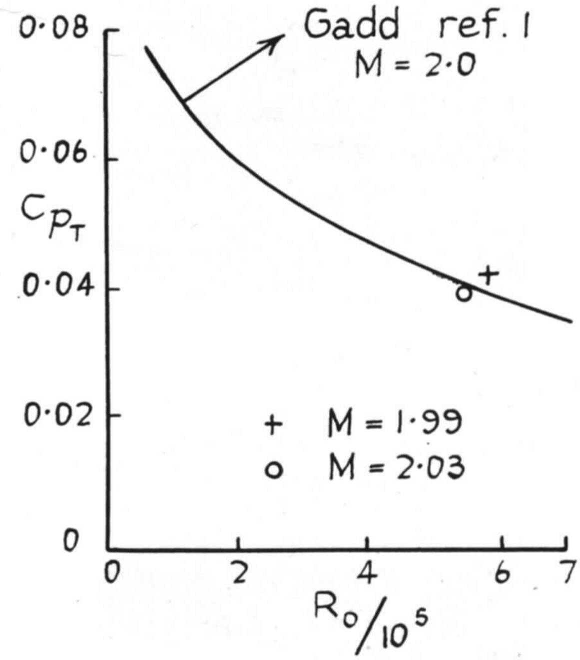

FIG. 4. Characteristics of the laminar foot. 12-deg double-wedge aerofoil results.

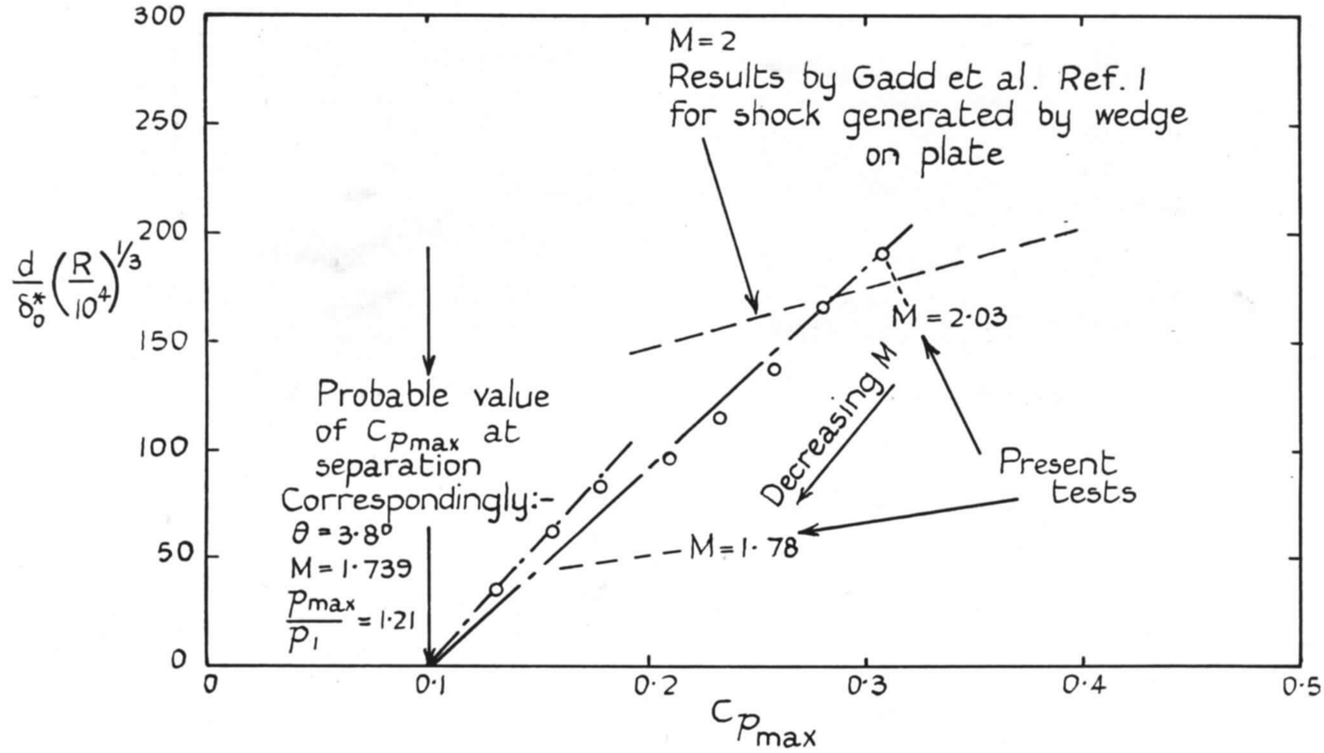

FIG. 5. First occurrence of separation for boundary layers laminar at separation and turbulent at reattachment. 12-deg double-wedge aerofoil results.

Fig. 6a. Laminar boundary layers.

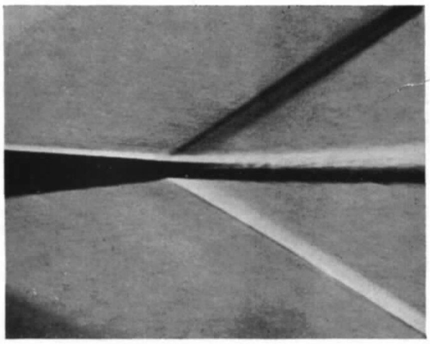

(i) $\theta = 4 \cdot 75$ deg.

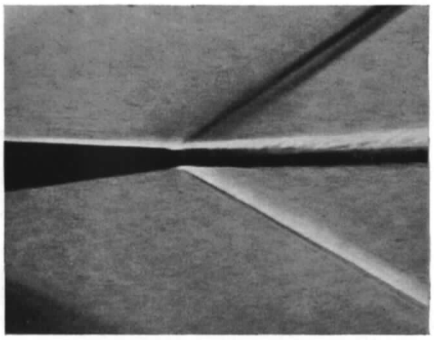

(ii) $\theta = 5$ deg.

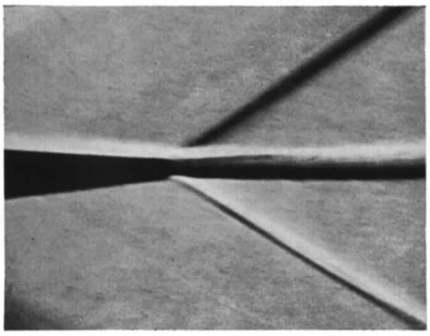

(iii) $\theta = 6$ deg.

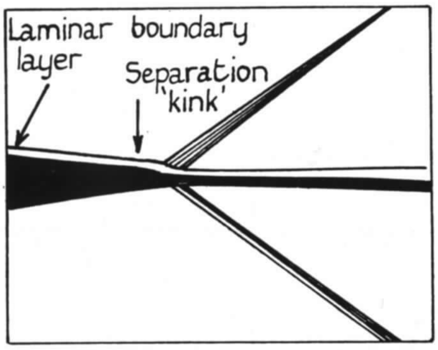

Fig. 6b. Turbulent boundary layers.

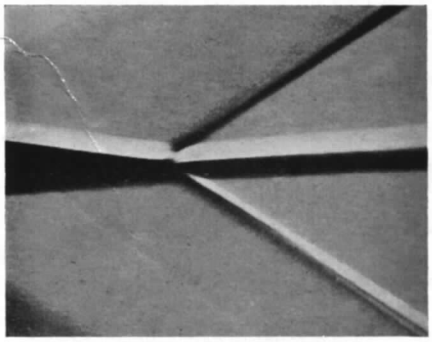

(i) $\theta = 12$ deg.

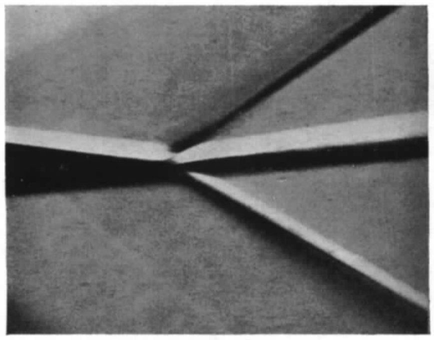

(ii) $\theta = 12\frac{1}{2}$ deg.

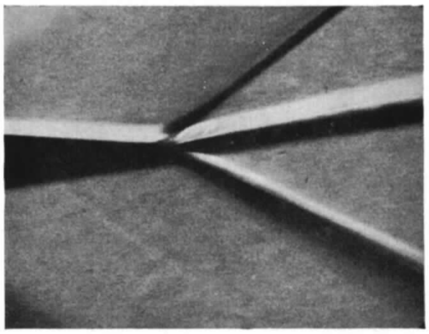

(iii) $\theta = 13$ deg.

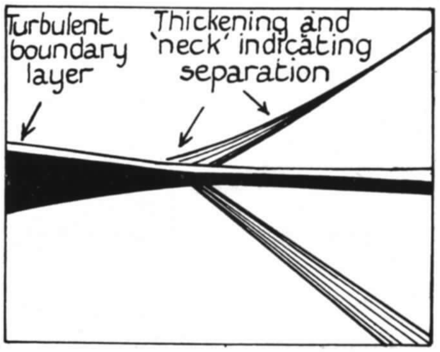

Fig. 6. 12-deg double-wedge aerofoil. First occurrence of boundary-layer separation. Schlieren photographs.

(4980) Wt. 20/9036 K.7 3/57 Hw.

PRINTED IN GREAT BRITAIN

Publications of the Aeronautical Research Council

ANNUAL TECHNICAL REPORTS OF THE AERONAUTICAL RESEARCH COUNCIL (BOUND VOLUMES)

1939 Vol. I. Aerodynamics General, Performance, Airscrews, Engines. 50s. (51s. 9d.).
Vol. II. Stability and Control, Flutter and Vibration, Instruments, Structures, Seaplanes, etc. 63s. (64s. 9d.)

1940 Aero and Hydrodynamics, Aerofoils, Airscrews, Engines, Flutter, Icing, Stability and Control Structures, and a miscellaneous section. 50s. (51s. 9d.)

1941 Aero and Hydrodynamics, Aerofoils, Airscrews, Engines, Flutter, Stability and Control Structures. 63s. (64s. 9d.)

1942 Vol. I. Aero and Hydrodynamics, Aerofoils, Airscrews, Engines. 75s. (76s. 9d.)
Vol. II. Noise, Parachutes, Stability and Control, Structures, Vibration, Wind Tunnels. 47s. 6d. (49s. 3d.)

1943 Vol. I. Aerodynamics, Aerofoils, Airscrews. 80s. (81s. 9d.)
Vol. II. Engines, Flutter, Materials, Parachutes, Performance, Stability and Control, Structures. 90s. (92s. 6d.)

1944 Vol. I. Aero and Hydrodynamics, Aerofoils, Aircraft, Airscrews, Controls. 84s. (86s. 3d.)
Vol. II. Flutter and Vibration, Materials, Miscellaneous, Navigation, Parachutes, Performance, Plates and Panels, Stability, Structures, Test Equipment, Wind Tunnels. 84s. (86s. 3d.)

1945 Vol. I. Aero and Hydrodynamics, Aerofoils. 130s. (132s. 6d.)
Vol. II. Aircraft, Airscrews, Controls. 130s. (132s. 6d.)
Vol. III. Flutter and Vibration, Instruments, Miscellaneous, Parachutes, Plates and Panels, Propulsion. 130s. (132s. 3d.)
Vol. IV. Stability, Structures, Wind Tunnels, Wind Tunnel Technique. 130s. (132s. 3d.)

Annual Reports of the Aeronautical Research Council—

1937 2s. (2s. 2d.) 1938 1s. 6d. (1s. 8d.) 1939–48 3s. (3s. 3d.)

Index to all Reports and Memoranda published in the Annual Technical Reports, and separately—

April, 1950 - - - - R. & M. 2600 2s. 6d. (2s. 8d.)

Author Index to all Reports and Memoranda of the Aeronautical Research Council—

1909—January, 1954 R. & M. No. 2570 15s. (15s. 6d.)

Indexes to the Technical Reports of the Aeronautical Research Council—

December 1, 1936—June 30, 1939	R. & M. No. 1850	1s. 3d. (1s. 5d.)
July 1, 1939—June 30, 1945	R. & M. No. 1950	1s. (1s. 2d.)
July 1, 1945—June 30, 1946	R. & M. No. 2050	1s. (1s. 2d.)
July 1, 1946—December 31, 1946	R. & M. No. 2150	1s. 3d. (1s. 5d.)
January 1, 1947—June 30, 1947	R. & M. No. 2250	1s. 3d. (1s. 5d.)

Published Reports and Memoranda of the Aeronautical Research Council—

Between Nos. 2251–2349	R. & M. No. 2350	1s. 9d. (1s. 11d.)
Between Nos. 2351–2449	R. & M. No. 2450	2s. (2s. 2d.)
Between Nos. 2451–2549	R. & M. No. 2550	2s. 6d. (2s. 8d.)
Between Nos. 2551–2649	R. & M. No. 2650	2s. 6d. (2s. 8d.)

Prices in brackets include postage

HER MAJESTY'S STATIONERY OFFICE

York House, Kingsway, London W.C.2; 423 Oxford Street, London W.1 (Post Orders: P.O. Box 569, London S.E.1) 13a Castle Street, Edinburgh 2; 39 King Street, Manchester 2; 2 Edmund Street, Birmingham 3; 109 St. Mary Street, Cardiff; Tower Lane, Bristol, 1; 80 Chichester Street, Belfast, *or through any bookseller.*

S.O. Code No. 23-3004

R. & M. No. 3004